Journal of Materials Chemistry A

ROYAL SOCIETY OF CHEMISTRY

PAPER

View Article Online
View Journal | View Issue

Cite this: J. Mater. Chem. A, 2023, 11, 12885

Composite membranes consisting of acidic carboxyl-containing polyimide and basic polybenzimidazole for high-temperature proton exchange membrane fuel cells

Erli Qu,[a] Geng Cheng,[a] Min Xiao,[a] Dongmei Han,[ab] Sheng Huang,[a] Zhiheng Huang,[a] Wei Liu,[a] Shuanjin Wang*[a] and Yuezhong Meng*[a]

A novel acid-base composite membrane consisting of acidic carboxyl-containing polyimide (PI-COOH) and basic polybenzimidazole (OPBI) was fabricated and employed as a high-temperature proton exchange membrane (HT-PEM). PI-COOH was used to prepare HT-PEMs for the first time. The PBI-based acid-base composite membranes and ordinary composite membranes were investigated to elucidate the correlation between the polymer structure and membrane properties, especially in situations where phosphoric acid (PA) is used. The results show that OPBI-xPI-COOH composite membranes (*x* represents the weight percentage of PI-COOH in the entire membrane) deliver high proton conductivities and superior PA retention due to the continuous hydrogen bond network between OPBI and PI-COOH. The OPBI-50PI-COOH composite membrane revealed a proton conductivity of 89 mS cm^{-1} under low PA uptake (109%). Compared to the linear OPBI and OPBI-40PI composite membrane, a single cell with a low PA-doped OPBI-50PI-COOH composite membrane presented superior durability and power density (463 mW cm^{-2}) at 160 °C and 0% relative humidity. In a short-term durability test of 369 h, the voltage attenuation rate was only 119 μV h^{-1}. These outstanding outcomes indicate that the obtained acid-base composite membranes can be considered as capable candidates for HT-PEMs with enhanced performance.

Received 15th November 2022
Accepted 16th January 2023

DOI: 10.1039/d2ta08904a

rsc.li/materials-a

10th Anniversary statement

Congratulations on the 10th anniversary of *Journal of Materials Chemistry A*! For the past few decades, environmentally friendly energy materials and technologies have indeed revolutionized our lives, and they currently play a pivotal role in managing the energy-environment nexus, which is key to a sustainable future. In this connection, the *Journal*, with its high standards and well-known reputation, has been the primary communication platform for all scientists in the world. Benefiting from the platform, our article entitled "Polymer electrolytes for lithium polymer batteries" (*Journal of Materials Chemistry A*, 2016, **4**, 10038–10069) has been cited over 800 times. We are interested in new types of sustainable energy materials and devices, improving the performance of green energy devices, and enabling new concepts for the conversion and storage of energy. In this regard, we contribute this article to celebrate this grand festival and hope our journal becomes even more popular.

1 Introduction

Currently, proton exchange membrane fuel cells (PEMFCs) have been proven to be one of the most promising sustainable power generation technologies. In particular, high-temperature proton exchange membrane fuel cells (HT-PEMFCs) utilized at low humidity (or no humidity) and high temperature (>120 °C) are used for eco-friendly energy conversion in automobiles and fixed equipment, and they are capable of enhancing the kinetics of oxygen reduction reactions, increasing CO resistance of the catalyst, and simplifying water/heat management systems.[1–5]

Considerable research has been conducted on proton exchange membranes (PEMs), which are the paramount unit of HT-PEMFCs.[6–8] High-performance PEMs must engage in high proton conductivity, and possess excellent thermo-mechanical stability and durability at elevated temperatures and low humidity (or under anhydrous conditions). Based on these practical principles, phosphoric acid (PA)-adsorbed polybenzimidazole (PBI) is considered to be the most mature and prospective PEM among various candidate membrane materials.[9–12] Nevertheless, higher PA doping amounts should be absorbed on behalf of acquiring higher proton conductivity, which often results in a severe decrease in mechanical strength

[a]The Key Laboratory of Low-carbon Chemistry & Energy Conservation of Guangdong Province, State Key Laboratory of Optoelectronic Materials and Technologies, School of Materials Science and Engineering, Sun Yat-sen University, Guangzhou 510275, China. E-mail: mengyzh@mail.sysu.edu.cn

[b]School of Chemical Engineering and Technology, Sun Yat-sen University, Zhuhai 519000, China

due to the plasticizing effect of PA.[13–15] Furthermore, this may bring about the loss of PA on account of its low molecular weight during the period of the long-term running of the cell and affect its overall performance. This problem may be conquered by generating interactions with PBI to promote proton conduction by means of substituting amphoteric polyacid for PA.[16–20] Therefore, PA-doped PBI-type PEMs are still facing many challenges in the process of achieving commercialization, such as attaining higher proton conductivity, additional optimal mechanical properties, and PA retention ability with increased stability.

In the past few years, several strategies, such as organic-inorganic hybrids,[21–23] chemically and physically cross-linked membranes,[24–26] and acid-base composite membranes,[27–30] have been investigated to enhance the overall performance of PBI as a PEM. Acid-base polymer blends containing an acidic polymer and a basic polymer have been found to be excellent candidates for acid-base blends. With the physical crosslinking between *N*-containing basic groups and acidic groups, hydrogen bonding was also envisaged, which can increase dimensional stability and proton conductivity by the construction of new proton transportation channels.

Over the last few years, different types of sulfonated aromatic polymer materials, including sulfonated polyarylene ether sulfone (SPAES),[31,32] sulfonated polyimide (SPI),[33] sulfonated polybenzimidazole (SPBI),[34,35] sulfonated polyether ether ketone (SPEEK),[36] sulfonated poly(fluorenyl ether ketone) (SPFEK),[37] and sulfonated polyether sulfone (SPES),[38] have been developed and applied in HT-PEMs due to their remarkable structural stability and mechanical strength. For instance, Ye *et al.*[39] reported noncovalent cross-linked membranes using one uracil-terminated telechelic sulfonated polyimide (SPI-U) and another adenine-based crosslinking agent (SMA-A) to form bio-complementary hydrogen bonding, and the modified composite membranes presented improved proton conductivity and more optimal antioxidant performance. However, the common feature of these materials is that their comprehensive properties are strongly dependent on the degree of sulfonation, and when the degree of sulfonation increases, the chemical and mechanical properties will deteriorate.[40]

Polyimide (PI) is a high-performance polymer material with a trapezoidal structure that possesses high mechanical strength, and outstanding thermal and chemical stability. Thus, it has been widely applied in engineering plastics, advanced composite materials, fibers, films, proton transfer membranes, coatings, microelectronics, and in other fields.[41–43] However, because many polyimides are insoluble in common organic solvents, it is difficult to directly process them for large-scale production. In this situation, it is necessary to first treat a polyamide acid, and then heat-treat it for imidization. On the contrary, excellent solubility in organic solvents has been observed for polyimides containing fluorinated or ether-bonded monomers, for example, 4,4'-(hexafluoroisopropylidene)diphthalic anhydride (6FDA) and 4,4′-oxydiphthalic anhydride (ODPA).[44] Because of the above-mentioned properties, there is considerable demand for copolymerized PIs with satisfactory solubility in organic solvents.

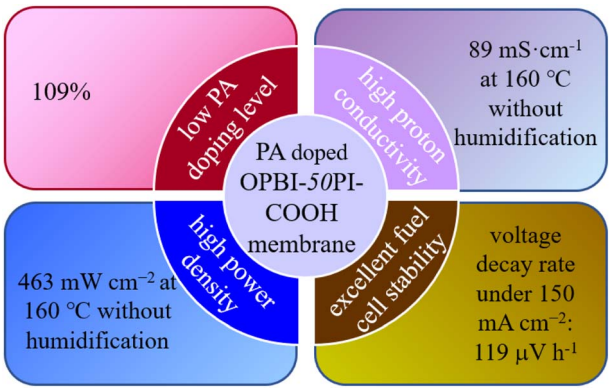

Fig. 1 Overview of the properties of PA-doped OPBI-50PI-COOH HT-PEMs.

In this work, PI with functional groups, *i.e.*, carboxyl groups, was prepared to form a high-molecular-weight acidic polymer (PI-COOH), which was used as a dopant for OPBI to form an acid-base polymer blend PEM with the capability to retain the proton transfer ability of OPBI under high temperatures and low humidity. The hydrogen bond network generated between the carboxylic acid group (–COOH) in PI-COOH and the imidazole group in OPBI can further prevent the leaching of low-molecular-weight PA, so as to increase the proton transport of the acid-base composite membranes through a hopping mechanism. Compared to the pristine linear OPBI, the as-prepared OPBI-50PI-COOH membrane presented higher proton conductivity under much lower PA-doping amounts. Moreover, it delivered improved H_2/O_2 single cell performance and excellent fuel cell stability (Fig. 1).

As far as we know, such a composite membrane has not been reported in the relevant literature or patents, implying its great potential as a HT-PEM. As a comparison, the proton conductivity, mechanical performance, thermal and antioxidative stabilities, and electrochemical performance of acid-base composite membranes between unfunctionalized PI and OPBI (OPBI-40PI) were also prepared and characterized as the control in this study.

2 Experimental

2.1 Materials

Poly[2,2′-(*p*-oxdiphenylene)-5,5′-benzimidazole] with a dynamic viscosity of 6000 Pa.S (OPBI) was supplied by Shanghai Shengjun Plastic Technology Co., Ltd. 3,5-Diaminobenzoic acid (DABA), 4,4'-(hexafluoroisopropylidene)diphthalic anhydride (6FDA), 4,4′-oxydianiline (ODA), 4,4′-oxydiphthalic anhydride (ODPA), phosphoric acid solution (85 wt%), and *N*,*N*-dimethylacetamide (DMAc) were supplied by Aladdin Chemical Co. Ltd.

2.2 Synthesis of soluble polyimide (PI) and acidic carboxyl-containing polyimide (PI-COOH)

A typical synthetic route for PI and PI-COOH was carried out using a two-step polycondensation reaction, as depicted in Scheme 1. The detailed preparation process is as follows.

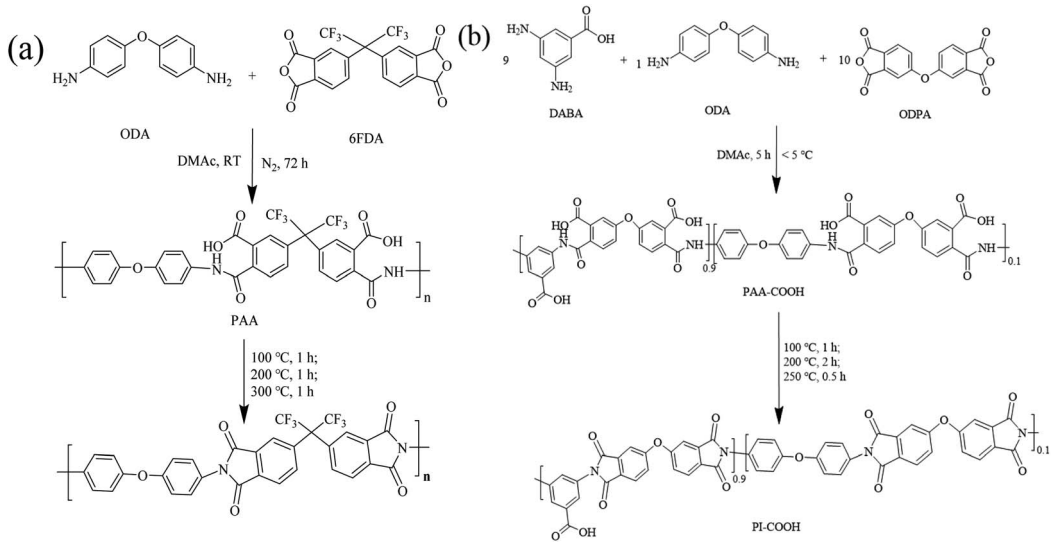

Scheme 1 Synthesis of PI-COOH and PI membranes.

2.2.1 PI membrane. In a 100 mL three-neck flask, ODA (1.20 g, 6 mmol) was added and dissolved with 30 mL DMAc by continuous magnetic stirring under nitrogen. Then, 6FDA (2.67 g, 6 mmol) was added in batches for mixed dissolution to control a solid content of 12 wt%. After the solid was dissolved, polyamide acid (PAA) was obtained after magnetic stirring for 72 h at room temperature. Then, the PAA membrane was formed by solution casting and volatilizing the solvent. Finally, the PAA membrane underwent thermal imidization using a muffle furnace at temperatures of 100 °C, 200 °C, and 300 °C for 1 h each to obtain the PI membrane. The chemical reaction process is shown in Scheme 1a.

2.2.2 PI-COOH membrane. Acidic carboxyl-containing polyimide (PI-COOH) was synthesized by introducing the diamino monomer of DABA containing carboxylic acid groups. The molar ratio of DABA to ODA was controlled at 9 : 1. First, DABA (1.37 g, 9 mmol) and ODA (0.20 g, 1 mmol) monomers were added to a 50 mL round-bottom flask containing 23 mL DMAc, and a transparent solution was then obtained by magnetic stirring at room temperature. After cooling to below 5 °C in an ice water bath, ODPA (3.10 g, 10 mmol) was gradually added. The solution was stirred for 5 h below 5 °C to acquire a viscous homogeneous transparent polyamide acid solution containing carboxylic acid (PAA-COOH) with a solid content of 20 wt%. The PAA-COOH solution was uniformly cast onto a clean glass sheet, and the solvent was removed at 80 °C for 6 h to form a PAA-COOH membrane. Finally, the PAA-COOH membrane was transferred to a muffle furnace for thermal imidization and treated step-by-step at 100 °C for 1 h, 200 °C for 2 h, and 250 °C for 0.5 h to form a light-yellow brown PI-COOH membrane. The synthesis of PI-COOH is shown in Scheme 1b.

2.3 Preparation of PI-COOH and OPBI acid-base composite membranes

As described in Scheme 2, the acid-base composite membranes composed of PI-COOH and OPBI in different proportions were prepared by dint using the solution casting method. The as-prepared membranes were named OPBI-*x*PI-COOH, where *x* denotes the weight percentage of PI-COOH in the composite membranes. In contrast, pure linear OPBI and OPBI-40PI composite membranes in Scheme 2 (40 represents the weight percentage of PI in the composite membrane, which is 40%) were also prepared. The preparation process is described as follows.

2.3.1 OPBI membrane. 1.0 g OPBI powder was dissolved in 10 mL DMAc by magnetic stirring for 12 h at 80 °C to form a homogeneous solution. The OPBI membrane was obtained by casting the cooled solution, and after volatilizing the solvent for 12 h at 80 °C, then drying it in an oven for 24 h at 100 °C.

2.3.2 OPBI-*x*PI-COOH acid-base composite membrane. Four OPBI-*x*PI-COOH membranes were prepared by acid-base blending of OPBI and PI-COOH at mass ratios of 5 : 5, 6 : 4, 7 : 3, and 8 : 2. The detailed preparation process of the OPBI-50PI-COOH membrane is illustrated below as an example, and the other ratio composite membranes were prepared in a similar manner. OPBI (0.29 g) powder was dissolved in 7 mL DMAc under vigorous magnetic stirring at 80 °C. Subsequently, the PI-COOH membrane was mixed with OPBI solution for 1 h at 80 °C. The OPBI-50PI-COOH membrane was formed by casting the mixed solution, and after volatilizing the solvent for 8 h at 60 °C, then drying it in an oven for 24 h at 100 °C.

2.4 Characterization

2.4.1 Characterization of the chemical structure. The chemical structure of PI and PI-COOH were analyzed *via* Fourier transform infrared (FT-IR) spectroscopy and ^{1}H nuclear magnetic resonance (NMR) spectroscopy. The FT-IR spectroscopy was performed using an attenuated total reflectance spectrometer (ATR-FT-IR, Scientific Nicolet 6700) over a wavenumber range of 4000–650 cm^{-1}. ^{1}H NMR spectroscopy were performed using a spectrometer (Bruker DRX-500), and tetramethylsilane (TMS) and deuterated dimethyl sulfoxide (DMSO-

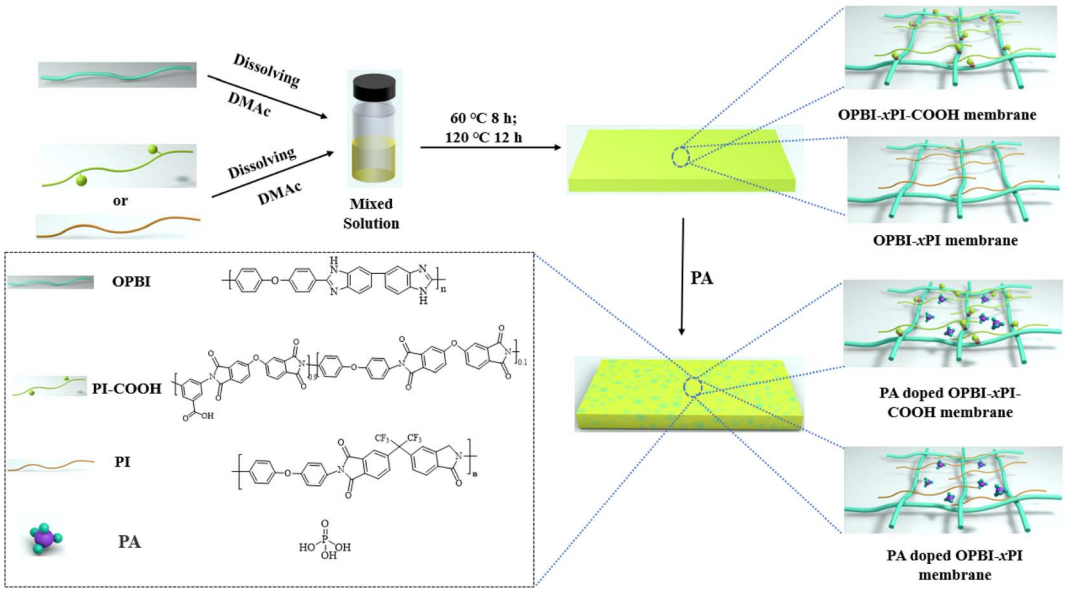

Scheme 2 Preparation of OPBI-*x*PI-COOH and OPBI-*x*PI membranes.

d_6) were used as the internal standard and solvent, respectively. The molecular weights of the synthesized PI and PI-COOH were measured by gel permeation chromatography (GPC) using a Waters 1515 isocratic HPLC pump, a Waters 717 plus autosampler, and a waters 2417 refractive index detector. Dimethylformamide (DMF) was used as the solvent at a flow rate of 1 mL min^{-1} at room temperature. The concentration of the polymer dissolved in DMF was 1 mg mL^{-1}.

2.4.2 Thermal stability. Thermogravimetric analysis (TGA) curves of membranes were obtained using a Pyris 1 TG instrument from PerkinElmer under a N_2 atmosphere. The samples were heated from room temperature to 800 °C at a rate of 10 °C min^{-1}.

2.4.3 Proton conductivity, PA uptake, and retention. The four-electrode AC impedance method was utilized to measure the proton conductivity of PA-doped membranes at different temperatures. An electrochemical workstation (AUT50992, AUTOLAB, 0.1 Hz-100 MHz) was employed to test the membrane's impedances. Conductivities were acquired from the change in direct current voltage between the two internal electrodes, which was performed from 80 °C to 180 °C without humidification. The conductivity σ (S cm^{-1}) was computed on the basis of eqn (1):

$$\sigma = \frac{L}{R \times W \times D} \quad (1)$$

where L (cm) refers to the distance between the electrodes, and W (cm) and D (cm) denote the width and depth of the membrane, respectively. R (Ω) values were obtained from the Nyquist plots.

The dry membranes were soaked in 85 wt% PA solution for 12 h at 120 °C. After removing the membrane from the PA solution, surplus PA was wiped from the surface of the membrane with tissue paper, and the corresponding weight was measured. At least three samples were obtained from each membrane, and the average value was calculated. The adsorption capacity of PA and the volumetric swelling ratio for membranes was measured by eqn (2) and (3):

$$\text{PA uptake } (\%) = \frac{W_1 - W_0}{W_0} \times 100 \quad (2)$$

$$\text{Swelling ratio } (\%) = \frac{V_1 - V_0}{V_0} \times 100 \quad (3)$$

where W_0 and W_1, V_0 and V_1 represent the dry membrane and PA-doped membrane weight and volume, respectively.

The PA retention of PA-doped membranes was measured by means of the water vapor method.[45] Relative membranes were placed in water vapor at 80 °C and 30% relative humidity for 36 h employing a programmable constant temperature and humidity testing machine, PT-2090DZ0, and the weights of PA-doped membranes were measured at 16 h, 28 h, 32 h, and 36 h. The PA retention rate of the membrane was computed according to eqn (4):

$$\text{PA retention } (\%) = \frac{W_R}{W_A} \times 100 \quad (4)$$

where W_R and W_A denote the weights of PA-doped membranes before and after the PA retention testing, respectively.

2.4.4 Mechanical testing. The mechanical strength of the produced membrane samples (width: 5–10 mm, length: 40–50 mm) was measured by a tensile strength testing machine (New SANS, Shenzhen, China) with an operating rate of 5 mm min^{-1} up to sample failure at room temperature. Each membrane was subjected to at least three parallel experiments.

2.4.5 Oxidative stability. The oxidative stabilities of entire membranes before and after PA adsorption were investigated with Fenton's reagent. PA undoped membranes were submersed in Fenton's reagent (3 wt% H_2O_2, 4 ppm Fe^{2+}) for 48 h at 80 °C. Afterwards, the membranes were extracted *via*

filtering, washed with distilled water, dried for 24 h at 120 °C, and weighed. To more closely match reliable fuel cell conditions, the oxidation stability of the PA-doped membranes was also tested. The procedure was conducted by setting a gradient every 0.5 h in Fenton's reagent to observe the time of membrane breakage. To ensure the accuracy of the results, experiments were conducted in parallel on three samples from each membrane. The oxidative stability (OS, %) was determined by the remanent weight after the dip using eqn (5).

$$\mathrm{OS}\,(\%) = W_3/W_2 \times 100 \quad (5)$$

where W_2 and W_3 denote the weight of the sample before and after immersion, respectively.

2.4.6 Single cell performance characterization. The membrane electrode assemblies (MEAs) directly contacted the gas diffusion electrodes (GDEs) with Pt catalyst (1 mg cm^{-2} Pt loading; the catalyst consisted of 40 wt% Pt and 15% PTFE as the binder) and PA-doped membranes in single cells without hot pressing. The single cell (active area/5 cm^2) was assembled by PET gaskets and two metallic polar plates containing single serpentine flow fields, in which they were fixed by two stainless steel plates. The single cell measurement was executed with gas flows of 80- and 160 mL min^{-1} for non-humidified H_2 and O_2 at 160 °C without backpressure, respectively.

Polarization curves were collected from a HT-PEMFC testing system by gradually controlling current densities from 0 (open circuit) to 1600 mA cm^{-2} or until the voltage dropped below 0.3 V. The short-term durability was also tested for PA-doped OPBI-50PI-COOH membrane fuel cells at an identical current density of 150 mA cm^{-2} operated at 140 °C without humidity or backpressure.

3 Results and discussion

3.1 Structural characterization of PI and PI-COOH

To obtain soluble polyimide polymers, the dianhydride monomers (6FDA and ODPA) and diamino monomer (ODA) containing flexible groups (–$C(CF_3)_2$– or O–) were used for PI and PI-COOH, respectively. A carboxylic acid group-containing diamino monomer (DABA) was used to copolymerize with ODA to synthesize PI-COOH. The molar ratio of DABA to ODA was controlled at 9 : 1 to produce an optimal interaction between PI-COOH and OPBI in the composite membranes.

With regard to the characterization of molecular weight correlation, the GPC results showed that the weight-average molecular weights of the synthesized PI and PI-COOH were 305 700 g mol^{-1} and 490 500 g mol^{-1}, respectively, suggesting that a high molecular weight was acquired. The structures of the synthesized PI and PI-COOH were confirmed by FT-IR spectroscopy. PI and PI-COOH generally represent specific vibrational bands, including C=N symmetrical stretching vibration, symmetric and asymmetric vibration of C=O, and deformation vibration from the imide five rings. As revealed in Fig. 2, for PI and PI-COOH, some distinct characteristic absorption peaks for imide appear at approximately 1791 cm^{-1} (imide asymmetric C=O stretching vibration), approximately 1714 cm^{-1} (imide symmetric C=O stretching vibration), approximately 1354 cm^{-1} (C-N stretching vibration), and approximately 722 cm^{-1} (deformation vibration from the imide five rings). The absorption band at approximately 1503 cm^{-1} denotes C=C bonds in aromatic rings, and the noticeable vibration band at approximately 1081 cm^{-1} was assigned to the ArO–Ar linkage structure. Additionally, both polymers exhibited a broadband absorption between 3200 cm^{-1} and 3700 cm^{-1}, which can be ascribed to the symmetrical stretching vibration of O–H from –COOH and H_2O.

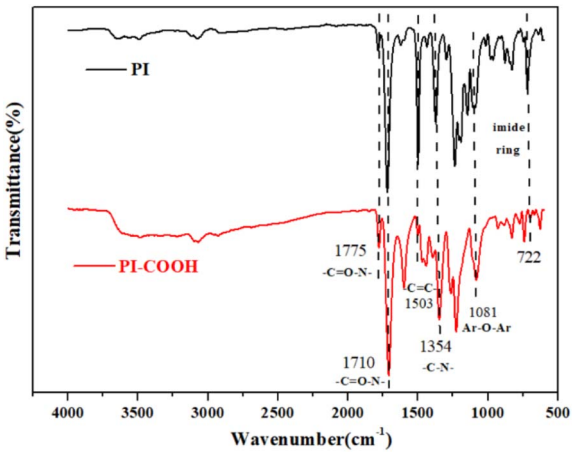

Fig. 2 FT-IR spectrum of PI and PI-COOH.

The ^{1}H NMR (500 MHz, DMSO-d_6) spectra of the prepared PI and PI-COOH are depicted in Fig. 3 to further confirm their structure. The chemical shift of the aromatic protons of both polyimides clearly appear at 7.0–8.5 ppm. Moreover, for PI-COOH, the hydrogen resonance signal of carboxylic acid groups is at 13.5 ppm. According to the data analysis of the FT-IR and NMR spectra, both polyimides were successfully synthesized.

3.2 Thermal stability

TGA was used to measure the thermal stability of OPBI-*x*PI–COOH–10% blend membranes under a N_2 atmosphere at

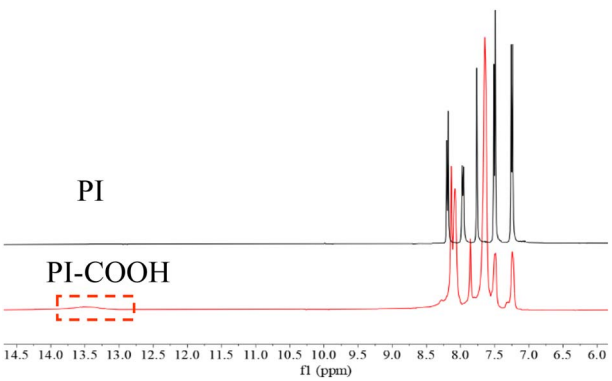

Fig. 3 ^{1}H NMR spectra of PI-COOH (in red) and PI (in black) in DMSO-*d*6.

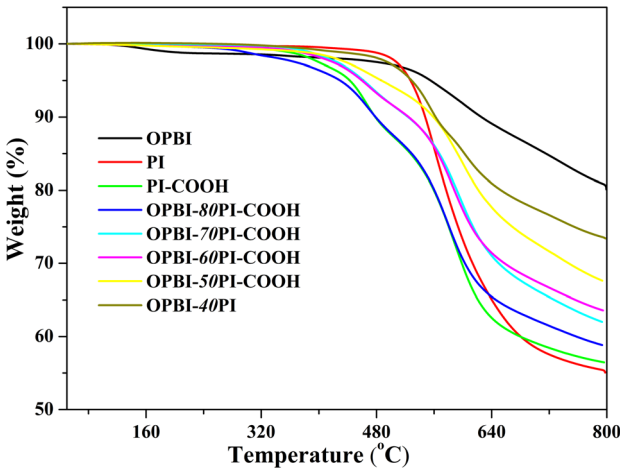

Fig. 4 TGA curves of all the membranes under N_2 atmosphere at a heating rate of 10 °C min^{-1}.

a heating rate of 10 °C min^{-1}. As represented in Fig. 4, the PI-COOH and OPBI-*x*PI-COOH composite membranes decomposed in two stages. In terms of the PI-COOH membrane, the first weight loss at 400 °C or so is ascribed to the disintegration of carboxyl acid groups, while the second major weight loss at approximately 500 °C results from the decomposition of the main chains of PI-COOH. For the OPBI-*x*PI-COOH composite membranes, the addition of PBI can lead to decomposition at higher temperatures regardless of the presence of carboxyl acid groups or PI-COOH main chains. Furthermore, with increasing OPBI content, the residual free carboxyl acid groups decreased due to the acid-base interaction between the carboxyl acid group and the active sites (–NH– and –N = groups) on the imidazole ring. Therefore, the first step becomes decreasingly obvious or even disappears when the weight percentage ratio of OPBI increases from 20% to 50%.

It is noteworthy that the TG curve of OPBI-*x*PI-COOH is significantly inconsistent with OPBI-0.4PI. With regard to the latter, its degradation trend and platform are nearly the same as that of the pure PI membrane. The reason for this is because there is no internal interaction between PI and OPBI, which results in poor stability of the OPBI-0.4PI composite membrane. These results imply that the thermal stability of the OPBI-*x*PI-COOH composite membranes is superior to that of pure PI-COOH. Moreover, the greater the amount of OPBI, the stronger the acid-base internal interaction, *i.e.*, the greater the stability. In addition, the temperatures at 5% weight loss ($T_{-5\%}$) for each sample from the TG curves are all greater than 400 °C, which shows that they can meet the application requirements of HT-PEMs.

3.3 Proton conductivity, PA uptake, and retention

Fig. 5a compares the temperature dependence of the proton conductivity for different PA-doped membranes without humidification. The results show that the proton conductivity is positively correlated with temperatures between 80 °C and 160 °C, whereas the slight decrease above 160 °C is mainly

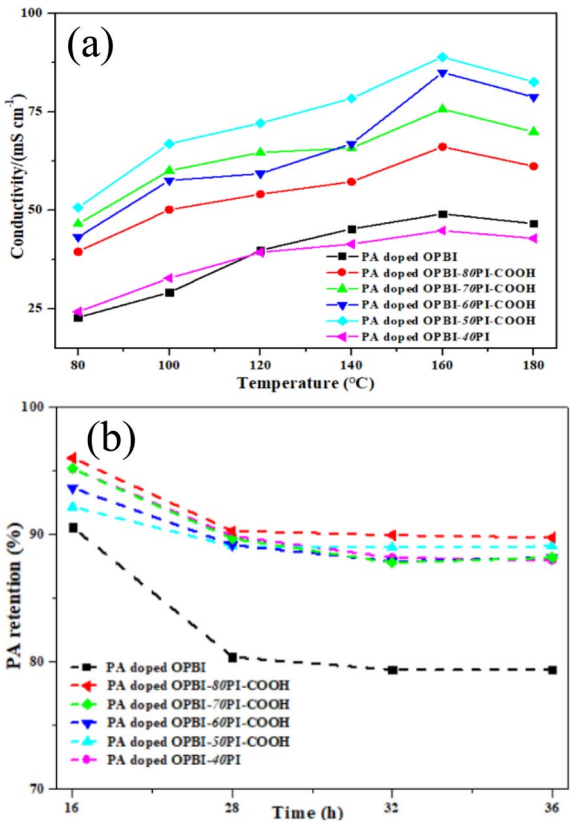

Fig. 5 (a) Proton conductivity plots of PA-doped OPBI, OPBI-*x*PI-COOH. and OPBI-40PI membranes at different temperatures without humidification; (b) PA retention of PA-doped OPBI, OPBI-*x*PI-COOH, and OPBI-40PI membranes at 80 °C with 0% relative humidity.

dependent on the dimerization of PA.[46] Significantly, as it is clear in Fig. 5a, the PA-doped OPBI-*x*PI-COOH composite membranes exhibited higher conductivities than the PA-doped OPBI and OPBI-40PI membranes on the basis of the same test criteria.

Table 1 shows the proton conductivities and volume swelling ratios of the PA-doped membranes at 160 °C. Interestingly, the proton conductivity of the OPBI-50PI-COOH acid-base composite membrane with 109% PA uptake was as high as 89 mS cm^{-1}, which is superior to that of the OPBI membrane with 250% PA uptake (49 mS cm^{-1}). Moreover, the volumetric swelling ratios of the OPBI-50PI-COOH composite membrane were reduced to only 34% of that of OPBI, and high proton conductivity continued. This realizes the goal of higher proton conductivity of the membrane at lower PA adsorption capacity, which can alleviate the deterioration of cell performance caused by loss of excessive free PA.

For HT-PEMFC systems with PA as the medium, once the acid overflows, it cannot be retrieved. Under long-term operation, PA loss may occur because of the formation of water at the cathode end. Therefore, the retention capacity of PA is critical to maintaining the performance of PEMs. PA leaching tests were carried out to identify their retention, and PA retention of all the PA-doped membranes is shown in Fig. 5b. According to the calculation results at different times, it can be concluded that

Table 1 Proton conductivities (δ) of different PA-doped membranes

Sample	PA uptake/%	S_{volume} (%)	Proton conductivity/mS cm^{-1} (160 °C)
PA-OPBI	250.0	128 ± 12	49
PA-OPBI-40PI	145.0	50 ± 2	45
PA-OPBI-80PI-COOH	41.0	12 ± 2	66
PA-OPBI-70PI-COOH	85.7	25 ± 5	76
PA-OPBI-60PI-COOH	86.4	27 ± 7	85
PA-OPBI-50PI-COOH	109.0	43 ± 4	89

there was more rapid PA loss in all the PA-doped membranes during the first 16 h, with stability at 28 h, and the difference was small compared with 36 h. It should be noted that the composite membranes presented much higher PA retention, compared to the neat OPBI membrane.

The above results are considered to be caused by the intermolecular interaction among the nitrogen groups of PBI, carboxyl acid groups, and free PA. The active nitrogen sites (–NH– and –N═ groups) of the imidazole ring in the OPBI skeleton play a vital role in such phenomenon, because nitrogen can serve as a proton donor and acceptor, promoting proton conduction by a Grotthuss-type mechanism *via* acid-base intermolecular interaction without humidification. Also, the proton conductivity increases with the increase in the OPBI content, which further demonstrates the formation of a more continuous hydrogen bond network that will facilitate proton transport and high PA retention.

The possible proton transport mechanism for OPBI-*x*PI-COOH membranes under anhydrous conditions is revealed in Scheme 3, where the proton exchange between ═NH$^+$– on the OPBI backbone and -COO$^-$ carboxylate groups on the PI-COOH is helpful for the transport of protons through the Grotthuss mechanism. At the same time, the intermolecular proton jumping occurring between acidic –COOH groups of PI-COOH also facilitates the movement of protons within membranes.

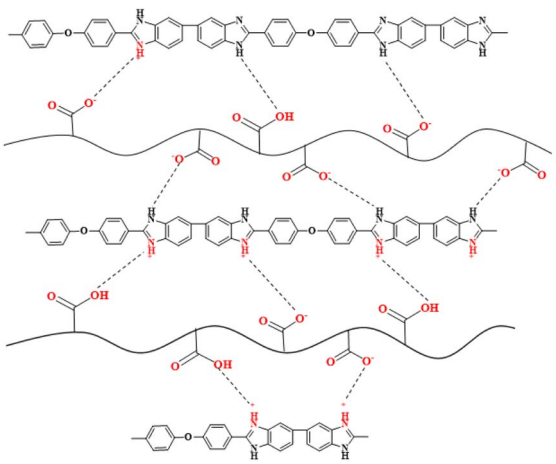

Scheme 3 Proposed proton transporting mechanism for OPBI-*x*PI-COOH membranes.

3.4 Mechanical and oxidative stability

The excellent mechanical performance and chemical stability of the PA-doped membranes are necessary for cell operation. The stress–strain curves of membranes are illustrated in Fig. 6. The tensile strengths of the PA-doped OPBI-*x*PI-COOH composite membranes increase with the increasing OPBI content. The mechanical strength of the PA-doped OPBI-*50*PI-COOH membrane is comparable to that of the PA-doped OPBI membrane, and it is assigned to the generation of hydrogen bond interactions. The existence of PI-COOH results in disarray in the OPBI chains, and the generation of hydrogen bonds between the –N═(or –NH–) groups of OPBI and the –COOH group of PI-COOH enhances the blended cohesion.[47] These parameters are adverse and balance out their influence, and thus no obvious change in tensile strength was viewed between PA-doped OPBI-50PI-COOH and the OPBI membranes. For the PA-doped OPBI-40PI composite membrane, its sturdiness was derived from the addition of high-strength PI. These results imply that the mechanical properties of OPBI-*x*PI-COOH composite membranes are strengthened by the increase in OPBI content due to the acid-base interaction, which assists in the utilization of the membrane under acidic operating conditions.

Another pivotal factor that affects the performance of HT-PEMs is the oxidative stability. As given in Fig. 7, the oxidative stability of the OPBI-50PI-COOH composite membrane is slightly poorer than that of the OPBI membrane. The

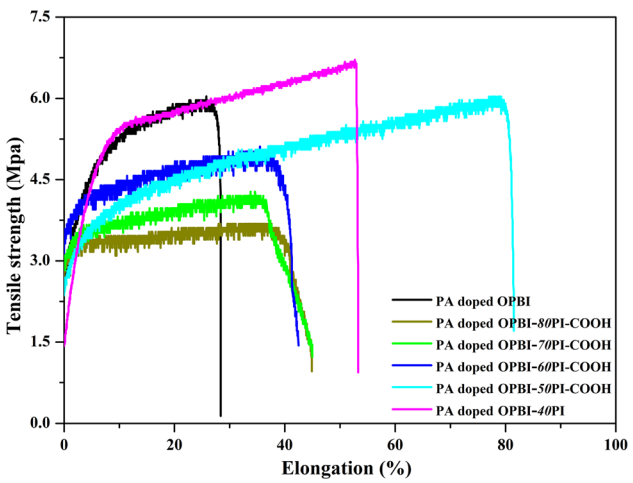

Fig. 6 Stress–strain curves of the different PA doped membranes.

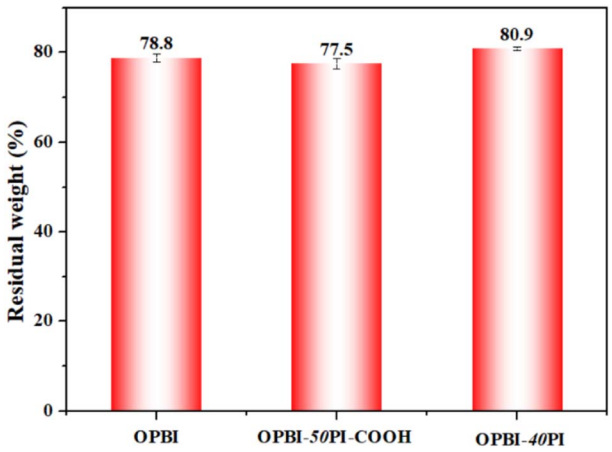

Fig. 7 Residual weights of the membranes after treatment in Fenton's reagent for 48 h at 80 °C.

Table 2 Elapsed time for all PA-doped membranes to begin to break into pieces

Sample	Time/h
PA-OPBI	2.0
PA-OPBI-80PI-COOH	2.5
PA-OPBI-70PI-COOH	4.0
PA-OPBI-60PI-COOH	6.0
PA-OPBI-50PI-COOH	7.0
PA-OPBI-40PI	2.5

aforementioned results are attributed to the high hydrophilicity of PI-COOH and its poor chemical stability as a result of the attack of hydroperoxyl and hydroxyl free radicals (˙OOH and ═OH) because of the presence of its ether bonds and carboxyl groups. Similarly, OPBI-40PI composite membranes also exhibited a similar phenomenon. Table 2 presents the elapsed time for all PA-doped membranes to begin to break into pieces, and the PA-doped composites exhibit increased antioxidant stability. The data show that the oxidative stability of PA-doped membranes is the result of the combined effect of PA adsorption and mechanical properties, which is also consistent with our previous research.[48]

3.5 HT-PEM fuel cell performance

The fuel cell performances of PA-doped membranes were investigated at 180 °C without humidification, and the matching polarization curves are depicted in Fig. 8a. As shown in Fig. 8a, the OPBI-50PI-COOH composite membrane displayed a superior fuel cell performance as compared to the OPBI and OPBI-40PI membranes. The OPBI-50PI-COOH composite membranes with lower PA uptake (109%) exhibited a high peak power density of 463 mW cm^{-2} with a flow rate of 80- and 160 mL min^{-1} for non-humidified H_2 and O_2 without backpressure, respectively. However, under the same testing conditions, the pure OPBI and OPBI-40PI membranes with higher PA uptake (250% and 145%) delivered only 422 mW cm^{-2} and 402 mW

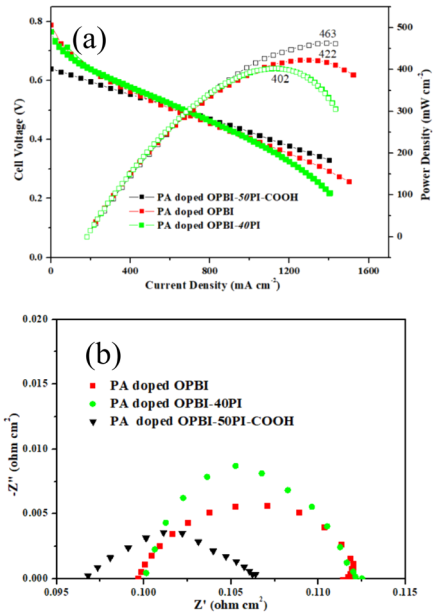

Fig. 8 (a) Polarization and power density profiles of PA-doped membranes for HT-PEMFCs at 160 °C, and (b) *in situ* impedance spectra of the MEAs with different PA-doped membranes at a cell voltage of 0.7 V and 160 °C.

cm^{-2} of the peak power density, respectively. Indeed, the formation of hydrogen bond interactions between OPBI and PI-COOH contributed to increased proton conductivity and high PA retention, which then enhanced the fuel cell performance. The comparison of the power density indicates that the obtained OPBI-50PI-COOH acid-base composite membrane is a promising candidate PEM for HT-PEMs.

To further analyse the influence of different feature combinations on the electrochemical reaction performance of the MEA, the impedance of a single cell was tested at a voltage of 0.7 V (Fig. 7b). The Nyquist diagram shows that a decrease in the high-frequency resistance (HFR) at 0.7 V follows the trend of PA-doped OPBI-40PI membrane > PA-doped OPBI membrane > PA-doped OPBI-50PI-COOH membrane. This indicates that the lower HFR of the MEA with the PA-doped OPBI-*50*PI-COOH membrane can be assigned to increased proton transfer resulting from the use of PEM, with consequently a lower proton transport resistance. The lowest charge transfer resistance (R_{CT}) was achieved by the MEA with a PA-doped OPBI-50PI-COOH membrane, which is consistent with the polarisation and power density curves in Fig. 8a.

For the purpose of assessing the working stability of the PA-doped composite membrane fuel cell, the short-term durability of constant current discharge for the PA-doped OPBI-50PI-COOH membrane with optimal comprehensive performance was tested by a startup/shutdown procedure, as shown in Fig. 9a. The cell experienced a rapid voltage drop in the first 24 h short-term durability test, which may have been caused by the redistribution of PA in the membrane electrode[49] and the agglomeration of Pt catalyst nanoparticles.[50] The distribution of PA in the membrane electrode subsequently reached

equilibrium, thus exhibiting a stable discharge behaviour, which is in accordance with the results for the PA retention rate.

Additionally, the working voltage of a single cell with PA-doped OPBI (1.0 mV h^{-1}) and OPBI-40PI membranes (1.2 mV h^{-1}) rapidly decreased, and the attenuation rate was approximately 2 times that of the PA-doped OPBI-50PI-COOH membrane (0.56 mV h^{-1}) during the stability test of 50 h. This further indicates that the addition of PI-COOH can lengthen the working lifetime of a single cell with a PA-doped OPBI-based membrane. Moreover, the working voltage decay rate of the PA-doped OPBI-50PI-COOH membrane HT-PEMFC was 119 μV h^{-1} during the stability test of 369 h. Remarkably, the voltage can be restored to the same level as that during the initial state after each shutdown/startup procedure. That is, the performance of the PA-doped OPBI-50PI-COOH membrane HT-PEMFC was not affected by a shutdown during the different stages, indicating that the PA-doped OPBI-50PI-COOH membrane possesses admirable stability.

The peak power densities of the PA-doped OPBI-50PI-COOH membrane fuel cell at different operating times are shown in Fig. 9b. The peak power densities decrease from the initial 456 mW cm^{-2} to 441 mW cm^{-2} after 117 h, and the calculated

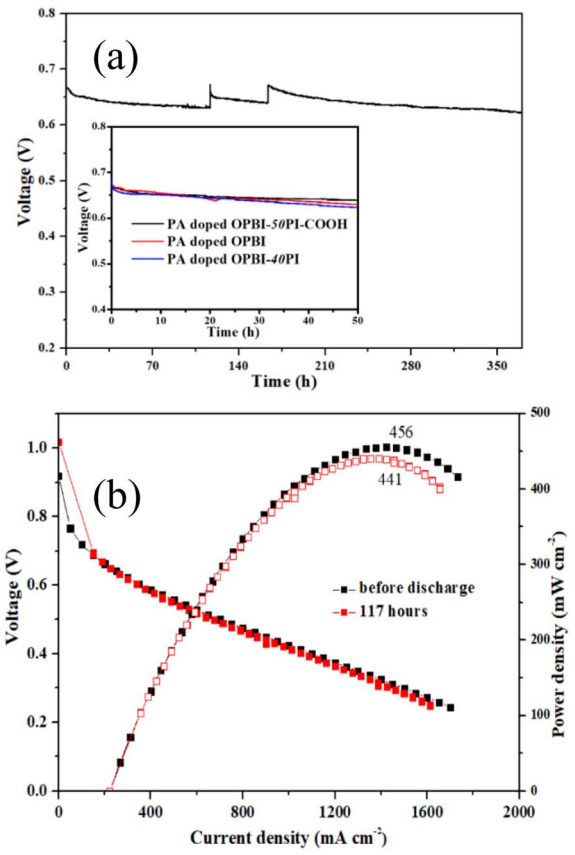

Fig. 9 (a) Short-time durability test of a PA-doped membrane fuel cell with an identical current density of 150 mA cm^{-2} operated without humidity and backpressure at 140 °C; (b) polarization and power density curves at different operating times for cells with a PA-doped OPBI-*50*PI-COOH membrane at 140 °C with gas flows of 80- and 160 mL min^{-1} for dry H_2 and O_2 without backpressure.

Table 3 Summary comparison of the main performance of PBI-based HT-PEMs previously reported and in this work

	Membrane parameter		Fuel cell performance				
Membrane type	PA uptake (%)	Proton conductivity (mS cm^{-1}) (*T*/°C, RH/%)	Voltage (V) *vs.* H_2/O_2 (Pt mg^{-1} cm^{-2}, *T*/°C, RH/%)	Voltage decay rate (μV h^{-1}) (approximate duration per h, current density per mA cm^{-2})	Maximum power density (%) (*T*/°C, RH/%)	Ref.
OPBI-50PI-COOH	109	89 (160, 0%)	0.92 (0.4, 140, 0)	119 (369, 150)	456 (140, 0)	This work
PBI	210	—	0.73 (0.4, 150, 0)	676 (182, 200)	290 (125, 0)	51
PBI	95	—	- (Cathode: 0.75& Anode:1.0, 160, 0)	363 (70, 300)	—	52
Asymmetrically porous PBI	307	82 (160, 0%)	0.86 (0.2, 160, 0)	283 (720, 200)	835 (160, 0)	53
PES-PVP-NH	245	152 (180, 5)	0.9 (0.26, 160, 0)	1400 (120, 200)	480 (180, 0)	54
6-*c*-sTiO_2-PBI-OO (6 wt% sTiO_2)	392	98 (160, 5)	~1.0 (0.47, 160, 0)	98 (300, 200)	356 (160, 0)	55
SC-B-OPBI-10	223	44 (180, 0)	0.94 (0.4, 160, 0)	110 (200, 200)	404 (160, 0)	56
Symmetric sponge-like porous OPBI	545	71 (180, 0)	0.86 (0.65, 160, 0)	Poor durability (~72, 300)	485 (160, 0)	57
PSf-TEA-110	238	78 (160, 0)	~0.60 (0.65, 160, 0)	Poor durability (<30, 300)	~400 (160, 0)	58
m-PBI/1%CeO_2/g-C_3N_4	331	48 (140, 0)	0.94 (0.65, 160, 0)	188 (160, 300)	504 (160, 0)	59

attenuation rate was approximately 3.3%, which also suggests that its stability is excellent. Overall, the integral performance of the novel acid-base polymer composite membranes in this work is superior to that of the HT-PEMs listed in Table 3, with lower PA adsorption, higher proton conductivity, and superior single cell performance and stability. The above results demonstrate the promising application of the OPBI-*50*PI-COOH membrane for HT-PEMFCs.

4 Conclusions

In this work, PI-COOH with carboxyl functional groups was prepared and blended with OPBI for application as HT-PEMs. Some crucial performance indicators were characterized, including thermo-chemical stability, mechanical property, proton conductivity, PA uptake, and single cell performance. The OPBI-*50*PI-COOH acid-base composite membrane exhibited remarkable proton conductivity under lower PA uptake. The continuous hydrogen bond network between OPBI and PI-COOH promoted proton transport and resulted in high proton conductivity. In comparison with the neat OPBI, the OPBI-*50*PI-COOH acid-base composite membrane with low uptake (109%) displayed a power density of up to 463 mW cm^{-2} and proton conductivity of 89 mS cm^{-1} at 160 °C without humidification. Moreover, it exhibited excellent stability in short-term durability tests for HT-PEMFCs. The integral performance of the as-prepared acid-base composite membrane was far superior to that of HT-PEMs as recently reported, and was characterized by lower PA adsorption, higher proton conductivity, and more optimal single cell performance and stability, thus demonstrating that it is a promising candidate for HT-PEMFC application.

Conflicts of interest

There are no conflicts to declare.

Acknowledgements

This work was supported by the National Key Research and Development Program (2018YFA0702002), and the National Key Research and Development Program (Japan-China Joint Research Program) (2017YFE0197900).

References

1 A. A. Tahrim and I. N. H. M. Amin, *J. Appl. Membr. Sci. Technol.*, 2018, **23**, 37–62.
2 J. Fang, X. Lin, D. Cai, N. He and J. Zhao, *J. Membr. Sci.*, 2016, **502**, 29–36.
3 S. Rahman, M. S. Masdar, M. I. Rosli, E. H. Majlan, T. Husaini, S. K. Kamarudin and W. Daud, *Renewable Sustainable Energy Rev.*, 2016, **66**, 137–162.
4 P. Sun, Z. Li, F. Dong, S. Wang, X. Yin and Y. Wang, *Int. J. Hydrogen Energy*, 2017, **42**, 486–495.
5 Z. Xia, L. Ying, J. Fang, Y. Y. Du, W. M. Zhang, X. Guo and J. Yin, *J. Membr. Sci.*, 2017, **525**, 229–239.
6 F. Altaf, R. Gill, R. Batool, M. Drexler and K. Jacob, *Eur. Polym. J*, 2019, **110**, 155–167.
7 K. Hooshyari, H. Rezania, V. Vatanpour, P. Salarizadeh and M. Enhesari, *J. Membr. Sci.*, 2020, **612**, 118436–118451.
8 E. Qu, X. Hao, M. Xiao, D. Han, S. Huang, Z. Huang, S. Wang and Y. Meng, *J. Power Sources*, 2022, **533**, 231386–231405.
9 D. Chen, S. Yu, X. Liu and X. Li, *J. Power Sources*, 2015, **282**, 323–327.
10 K. Hooshyari, M. Javanbakht and M. Adibi, *Electrochim. Acta*, 2016, **205**, 142–152.
11 K. Hooshyari, M. Moradi and P. Salarizadeh, *Int. J. Energy Res.*, 2020, **44**, 2617–2633.
12 M. Ja Van Bakht, Z. Rajabi, K. Houshyari, A. Badiei and M. Adibi, *New J. Chem.*, 2020, **44**, 5001–5018.
13 M. Hazarika and T. Jana, *ACS Appl. Mater. Interfaces*, 2012, **4**, 5256–5265.
14 S. Maity and T. Jana, *Macromolecules*, 2013, **46**, 6814–6823.
15 J. Jiang, Z. Li, M. Xiao, S. Wang, K. Miyatake and Y. Meng, *J. Membr. Sci.*, 2022, **660**, 120878–120886.
16 U. Sen, O. Acar, A. Bozkurt and A. Ata, *J. Appl. Polym. Sci.*, 2011, **120**, 1193–1198.
17 E. Sevim ünügür, A. Bozkurt and S. S. Hosseini, *Prog. Polym. Sci.*, 2012, **37**, 1265–1291.
18 Z. Taherkhani, M. Abdollahi and A. Sharif, *Solid State Ionics*, 2019, **337**, 122–131.
19 Z. Taherkhani, M. Abdollahi and A. Sharif, *J. Electrochem. Soc.*, 2020, **167**, 104503–104513.
20 X. Hao, Z. Li, M. Xiao, D. Han, S. Huang, G. Xi, S. Wang and Y. Meng, *J. Mater. Chem. A*, 2022, **10**, 10916–10925.
21 S. Lee, K. Seo, R. V. Ghorpade, K. H. Nam and H. Han, *Mater. Lett.*, 2019, **263**, 127167–127171.
22 J. Yang, X. Li, C. Shi, B. Liu and B. Liu, *J. Membr. Sci.*, 2020, **620**, 118855–118864.
23 J. Zhang and S. P. Jiang, *Funct. Org. Hybrid Nanostruct. Mater.*, 2018, **10**, 383–418.
24 J. S. Yang, Q. F. Li, L. N. Cleemann, J. O. Jensen, C. Pan, N. J. Bjerrum and R. H. He, *Adv. Energy Mater.*, 2013, **3**, 622–630.
25 W. Li, B. Zla, L. Yi and W. Lei, *J. Membr. Sci.*, 2019, **583**, 110–117.
26 P. Ngamsantivongsa, H. L. Lin and T. L. Yu, *J. Polym. Res.*, 2016, **23**, 22–33.
27 G. A. Giffin, S. Galbiati, M. Walter, K. Aniol, C. Ellwein, J. Kerres and R. Zeis, *J. Membr. Sci.*, 2017, **535**, 122–131.
28 N. N. Krishnan, N. Duong, A. Konovalova, J. H. Jang and D. Henkensmeier, *J. Membr. Sci.*, 2020, **614**, 118494–118507.
29 B. Liu, Y. Zhang, Y. Jiang, P. Qian and H. Shi, *J. Membr. Sci.*, 2019, **591**, 117332–117739.
30 A. Zg, A. Mp, A. Jc, A. Zj and A. Smh, *J. Energy Chem.*, 2021, **63**, 393–429.
31 J. H. Chun, G. K. Sang, Y. L. Ji, H. H. Dong and K. T. Park, *Renewable Energy*, 2013, **51**, 22–28.
32 K. T. Park, J. H. Chun, G. K. Sang, B. H. Chun and S. H. Kim, *Int. J. Hydrogen Energy*, 2011, **36**, 1813–1819.
33 Z. J. Xia, H. Xu, X. X. Guo and J. H. Fang, *Adv. Mater. Res.*, 2011, **287–290**, 2516–2521.

34 I. Nicotera, V. Kosma, C. Simari, S. Angioni, P. Mustarelli and E. Quartarone, *J. Phys. Chem. C*, 2015, **119**, 9745–9753.
35 C. H. Shen, L. C. Hsu, E. Bulycheva and N. Belomoina, *J. Membr. Sci.*, 2012, **399–400**, 11–15.
36 Q. Rong, S. Gu, G. H. He, X. M. Wu, Z. W. Hu and X. M. Yan, *Polym. Mater.: Sci. Eng.*, 2009, 126–129.
37 Y. Bai, M. Xiao, Z. Huang, D. Han, C. Wang, S. Wang and Y. Meng, *J. Electrochem. Soc.*, 2021, **168**, 114509–114516.
38 S. Wen, C. Gong, W. C. Tsen, Y. C. Shu and F. C. Tsai, *Int. J. Hydrogen Energy*, 2009, **34**, 8982–8991.
39 Y. S. Ye, R. J. Huang, R. C. Cheng and R. C. Chang, *Chem. Commun.*, 2010, **46**, 7554–7556.
40 S. S. Lim, R. Wan, J. M. Jahim, M. Ghasemi, P. S. Chong and M. Ismail, *Int. J. Hydrogen Energy*, 2012, **37**, 11409–11424.
41 V. Narayanan, T. D. Dang, Z. W. Bai, V. K. McNier, J. N. DeCerbo, B. H. Tsao and J. T. Stricker, *Mater. Sci. Eng. B*, 2010, **168**, 16–21.
42 E. S. Weiser, T. F. Johnson, T. Clair, Y. Echigo and B. W. Grimsley, *High Perform. Polym.*, 2000, **12**, 1–12.
43 C. Zhao, W. Zhe, D. Bi, H. Lin, S. Ke, T. Fu, S. Zhong and N. Hui, *Polymer*, 2007, **48**, 3090–3097.
44 D. Düsselberg, D. Verreault, P. Koelsch and C. Staudt, *J. Mater. Sci.*, 2011, **46**, 4872–4879.
45 K. S. Lee, J. S. Spendelow, Y. K. Choe, C. Fujimoto and Y. S. Kim, *Nat. Energy*, 2016, **1**, 16120–16126.
46 W. Ma, C. Zhao, H. Lin, Z. Gang, N. Jing, W. Jing, W. Shuang and N. Hui, *J. Power Sources*, 2011, **196**, 9331–9338.
47 K. Hooshyari, H. Rezania, V. Vatanpour, R. Mohadese and H. R. Rajabi, *Int. J. Energy Res.*, 2021, 1–19.
48 E. Qu, J. Jiang, M. Xiao, D. Han, S. Huang, Z. Huang, S. Wang and Y. Meng, *Nanomaterials*, 2022, **12**, 773–789.
49 J. Hu, H. Zhang, Y. Zhai, L. Gang, J. Hu and B. Yi, *Electrochim. Acta*, 2007, **52**, 394–401.
50 J. Zhang, D. Aili, J. Bradley, H. Kuang, C. Pan, R. D. Marco, Q. Li and S. P. Jiang, *J. Electrochem. Soc.*, 2017, **164**, F1615–F1625.
51 F. J. Pinar, P. Canizares, M. A. Rodrigo, D. Ubeda and J. Lobato, *J. Power Sources*, 2011, **196**, 4306–4313.
52 D. Schonvogel, M. Rastedt, P. Wagner, M. Wark and A. Dyck, *Fuel Cells*, 2016, **16**, 480–489.
53 L.-C. Jheng, W. J.-Y. Chang, S. L.-C. Hsu and P.-Y. Cheng, *J. Power Sources*, 2016, **323**, 57–66.
54 J. Zhang, S. Lu, H. Zhu, K. Chen, Y. Xiang, J. Liu and M. Forsyth, *RSC Adv.*, 2016, **6**, 86575–86585.
55 N. N. Krishnan, S. Lee, R. V. Ghorpade, A. Konovalova, J. H. Jang, H. J. Kim, J. Han, D. Henkensmeier and H. Han, *J. Membr. Sci.*, 2018, **560**, 11–20.
56 M. Hu, J. Ni, B. Zhang, S. Neelakandan and L. Wang, *J. Power Sources*, 2018, **389**, 222–229.
57 K. Geng, H. Tang, Q. Ju, H. Qian and N. Li, *J. Membr. Sci.*, 2021, **620**, 118981–118988.
58 H. Tang, K. Geng, J. Hao, X. Zhang, Z. Shao and N. Li, *J. Power Sources*, 2020, **475**, 228521–228530.
59 B. Lv, K. Geng, H. Yin, C. Yang, J. Hao, Z. Luan, Z. Huang, X. Qin, W. Song and N. Li, *J. Membr. Sci.*, 2021, **639**, 119760–119769.